



Trans. Nonferrous Met. Soc. China 31(2021) 2074-2080

Transactions of Nonferrous Metals Society of China

www.tnmsc.cn



Facile synthesis of high capacity P2-type Na_{2/3}Fe_{1/2}Mn_{1/2}O₂ cathode material for sodium-ion batteries

Mu-lan QIN, Chang-yu YIN, Wen XU, Yang LIU, Jun-hao WEN, Bin SHEN, Wei-gang WANG, Wan-min LIU

Hunan Provincial Key Laboratory of Environmental Catalysis & Waste Recycling, College of Materials and Chemical Engineering, Hunan Institute of Engineering, Xiangtan 411104, China

Received 7 August 2020; accepted 8 April 2021

Abstract: P2-type $Na_{2/3}Fe_{1/2}Mn_{1/2}O_2$ was synthesized by a facile sol-gel method, and the effect of calcination temperature on the structure, morphology and electrochemical performance of samples was investigated. The results show that the sample obtained at 900 °C is pure P2-type $Na_{2/3}Fe_{1/2}Mn_{1/2}O_2$ phase with good crystallization, which consists of hexagon plate-shaped particles with the size and thickness of 2–4 μ m and 200–400 nm, respectively. The sample exhibits an initial specific discharge capacity of 243 mA·h/g at a current density of 26 mA/g with good cycling stability. The high specific capacity indicates that P2-type $Na_{2/3}Fe_{1/2}Mn_{1/2}O_2$ is a promising cathode material for sodiumion batteries.

Key words: sodium-ion battery; cathode material; Na_{2/3}Fe_{1/2}Mn_{1/2}O₂; electrochemical performance; sol–gel method

1 Introduction

Sodium-ion batteries (SIBs) are promising alternatives to lithium ion batteries for large-scale energy storage due to the abundant reserves and low cost of sodium [1-4]. Many materials have been reported as cathode materials for SIBs, such as layered transition metal oxides, hexacyanoferrate analogues and phosphate-based materials [5–8]. In particular, layered transition metal oxides with general composition of Na_rMeO₂ (Me is transition metal) have attracted considerable attention [9–12]. Sodium-based layered materials can be categorized into two main groups according to Delmas' classification: O3-type and P2-type, in which the sodium ions are accommodated at the octahedral and prismatic sites, respectively [13]. It has been recognized that the P2-type materials are more suitable as cathode for SIBs compared with O3-type materials because of their large interlayer spacing and high structural stability [14]. In these materials, the layered P2-type Na_{2/3}Fe_{1/2}Mn_{1/2}O₂ (hexagonal, *P*6₃/*mmc*) is regarded as one of the most promising cathode candidates. Its high theoretical specific capacity (260 mA·h/g) is of great potential for large-scale storage of electrical energy. In addition, all of the constituent elements (Na, Fe and Mn) are abundantly available and environment-friendly [15,16].

Layered P2-type Na_{2/3}Fe_{1/2}Mn_{1/2}O₂ as a cathode material for SIBs was first reported by YABUUCHI et al [17] with a specific discharge capacity of 190 mA·h/g, which now has been successfully prepared by solid state reaction [16,18,19], co-precipitation [20], electrospinning [21,22], sol—gel method [23–27], etc. However, the practical specific capacity, rate capability and cycle stability of P2-type Na_{2/3}Fe_{1/2}Mn_{1/2}O₂ are still unsatisfied, and most of the reported reversible capacities are less than 210 mA·h/g. Thus, further studies are necessary to

improve its electrochemical performances. In this work, the hexagon plate-shaped P2-type $Na_{2/3}Fe_{1/2}Mn_{1/2}O_2$ was synthesized, and its electrochemical performance was evaluated.

2 Experimental

2.1 Synthesis of P2-type Na_{2/3}Fe_{1/2}Mn_{1/2}O₂

All the reagents were of analytical grade and used as received. The hexagon plate-shaped P2-type Na_{2/3}Fe_{1/2}Mn_{1/2}O₂ was synthesized by a facile sol-gel method. In a typical process, stoichiometric quantities of NaNO₃, $Fe(NO_3)_3 \cdot 9H_2O$ Mn(CH₃COO)₂·4H₂O were dissolved in de-ionized water. Then, a citric acid solution was added into the obtained solution under continuous stirring with the molar ratio of total metal ions to citric acid kept as 1:1. The resulting solution was heated at 60 °C to remove the excess water and then further dried at 80 °C for 12 h to obtain a gel precursor. The precursor was ground finely and pre-calcined at 450 °C for 4 h in air, which was then calcined at 850, 900 and 950 °C for 10 h, respectively. After cooling to room temperature, the sample was collected immediately.

2.2 Characterization

The thermal decomposition process of the precursor was investigated by thermogravimetry (TG) and differential scanning calorimetry (DSC) using a simultaneous TG–DSC thermal analyzer (NETZSCH STA 449C) at a heating rate of 10 °C/min in air atmosphere. The X-ray power diffraction (XRD, Rigaku D/max 2500 with Cu K_{α} radiation) and scanning electron microscopy (SEM, SU 3500) were applied to characterizing the structure and morphology of obtained products, respectively.

2.3 Electrochemical measurements

The electrochemical properties of synthesized P2-type Na_{2/3}Fe_{1/2}Mn_{1/2}O₂ were evaluated via the coin cells (CR2025). Typically, P2-type Na_{2/3}Fe_{1/2}Mn_{1/2}O₂ active material, acetylene black and polyvinylidene fluoride (PVDF) binder were dispersed in N-methyl-2-pyrrolidone (NMP) solution in a mass ratio of 8:1:1 to make a slurry which was then coated on an Al foil and vacuum dried in an oven at 120 °C for 10 h to obtain the cathode. The assembly was performed in a glove

box using metallic Na as the anode, glass fiber (Whatman GF/D) as the separator and 1.0 mol/L NaClO₄ dissolved in ethylene carbonate (EC)-diethyl carbonate (DEC) (1:1 in volume) as the electrolyte. Cyclic voltammetry (CV) measurement was performed on a CHI660C electrochemical workstation at a scan rate of 0.1 mV/s. The galvanostatic charge—discharge characteristics of the cells were recorded with a Land battery tester (Land CT 2001A) and the specific capacity is based on the mass of active material only.

3 Results and discussion

3.1 Structure and morphology characteristics

The TG and DSC measurements were carried out to determine the thermal decomposition process and calcination temperature of the precursor, and the TG and DSC curves are shown in Fig. 1. On the TG curve, the mass loss of 18% before 130 °C is due to the removal of water molecule present in the precursor. The decomposition process mainly occurs in the temperature range of 130-450 °C. The mass loss of about 52% in temperature range of 130-450 °C is attributed to the complex decomposition of nitrates, citrates and acetates [28], and the DSC curve shows three distinguishable exothermic peaks at 132, 269 and 401 °C, respectively. There is no obvious mass loss at temperature higher than 600 °C, indicating that the decomposition of precursor is completed at 600 °C.

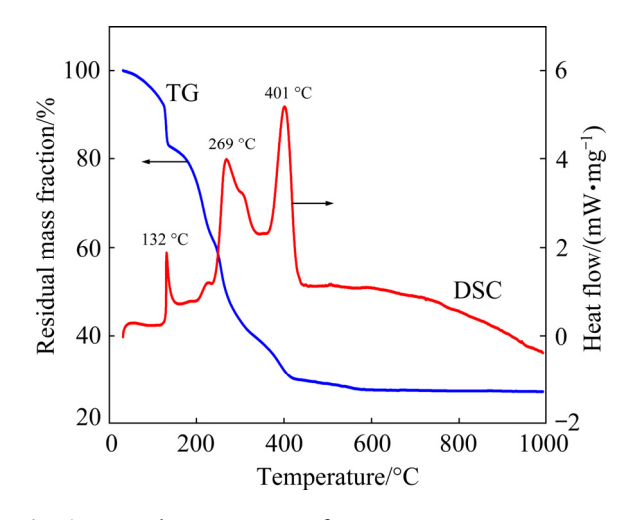


Fig. 1 TG and DSC curves of precursor

The phase structures of samples obtained at different temperatures were characterized by XRD. Figure 2 shows the XRD patterns of samples

synthesized at 850, 900 and 950 °C. It can be seen that all peaks of samples exhibit the characteristic diffraction peaks of P2-type $Na_{2/3}Fe_{1/2}Mn_{1/2}O_2$ without any miscellaneous phase, which are indexed to the hexagonal lattice with space group $P6_3/mmc$ [17,23,24]. In addition, By increasing the calcination temperature, the crystallinity of the samples increases and the main diffraction peaks become sharper.

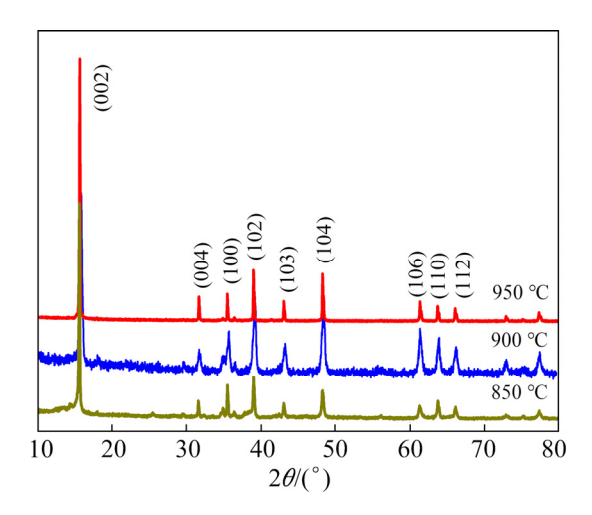


Fig. 2 XRD patterns of samples obtained at different temperatures

Figure 3 presents the SEM images of samples obtained at 850, 900 and 950 °C. It can be clearly seen that the particle size becomes larger as the calcination temperature increases. The sample obtained at 850 °C is composed of nanoparticles with a maldistribution of particle size, as shown in Fig. 3(a). With increasing the calcination temperature, the samples have a more uniform particle distribution and are composed of hexagon plate-shaped particles, as shown in Figs. 3(b, c). The size and thickness of sample calcined at 900 °C are in the range of 2-4 µm and 200-400 nm, respectively, and the thickness increases to 400-800 nm when calcining at 950 °C. The morphology of P2-type Na_{2/3}Fe_{1/2}Mn_{1/2}O₂ particles synthesized at 900 °C is closely similar to its crystal framework, indicating that the material is well crystallized, and the structure is stable in the charging and discharging process [16]. Moreover, the plates with sub-micro size are beneficial to shortening the ion diffusion distance and providing large contact area for electrochemical reactions, which can contribute to its good electrochemical performance.

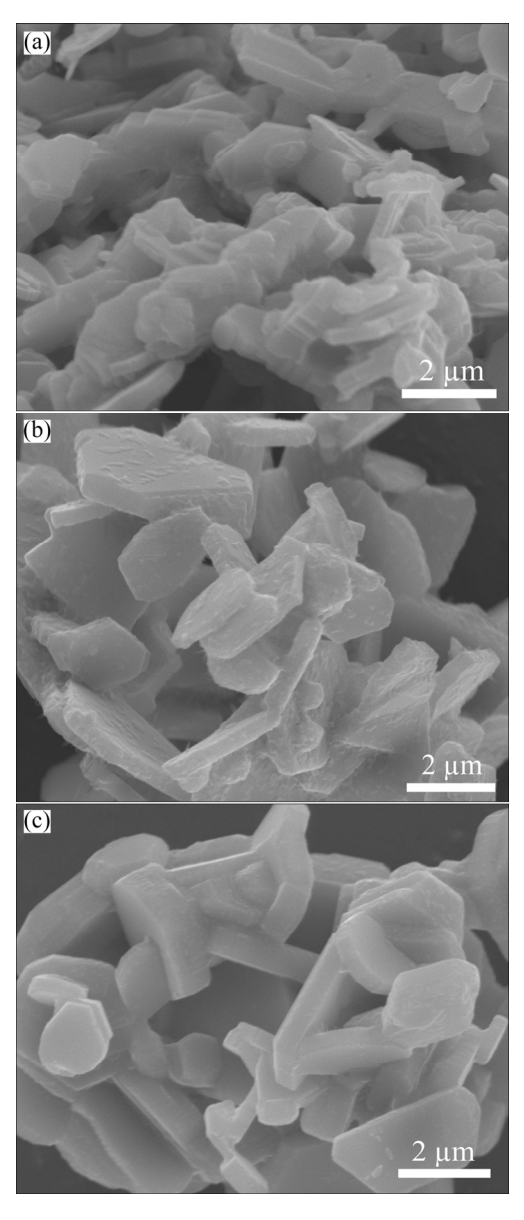


Fig. 3 SEM images of samples obtained at 850 $^{\circ}$ C (a), 900 $^{\circ}$ C (b) and 950 $^{\circ}$ C (c)

3.2 Electrochemical performance

The electrochemical performance of the cathode materials was evaluated using 2025-type coin cells. Figure 4 shows the CV curves of P2-type Na_{2/3}Fe_{1/2}Mn_{1/2}O₂ obtained at 900 °C in the voltage range of 1.5–4.2 V at a sweep rate of 0.1 mV/s. The CV curves are characterized by two pairs of redox current peaks. One at around 4.1/3.3 V corresponds to Fe³⁺/Fe⁴⁺ redox reaction and the other at 2.6/1.8 V is attributed to Mn³⁺/Mn⁴⁺ redox reaction [24,25,29]. There is a phase transition from P2-type (*P*6₃/*mmc*) to OP4-type (*P*6₃) after charging above 4.0 V, with the reverse phase transition from OP4-type to P2-type during the discharge

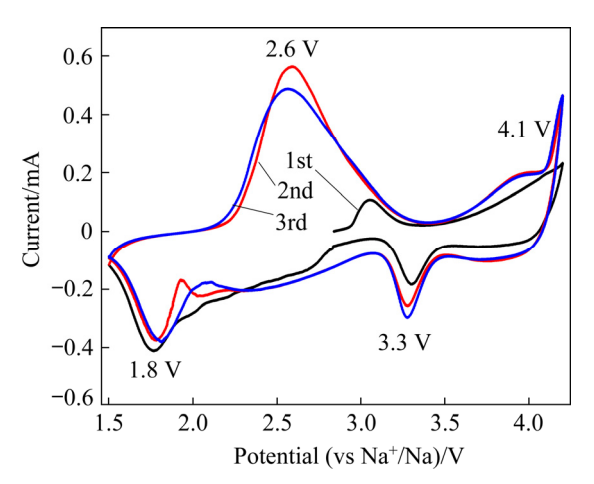


Fig. 4 CV curves of sample obtained at 900 °C

process [25,29]. When the coin cell is discharged below 2.0 V, the P2-type hexagonal phase transforms into a P2-type orthorhombic phase with *Cmcm* space group [24,30]. This complex phase/structure evolution can negatively affect the rate capability and cycling stability [19,24].

The first three charge-discharge curves of samples tested at a current density of 26 mA/g are shown in Figs. 5(a-c). On all curves, there are two charge plateaus at around 2.6 and 4.1 V, and two distinct discharge plateaus at around 3.3 and 1.8 V, which correspond well with the peak positions shown on the CV curves (Fig. 4). The initial specific discharge capacities of P2-type Na_{2/3}Fe_{1/2}Mn_{1/2}O₂ obtained at 850, 900 and 950 °C are 245, 243 and 155 mA·h/g, respectively. Figure 5(d) shows the cycling performance of samples obtained at different temperatures. The specific discharge capacities of P2-type Na_{2/3}Fe_{1/2}Mn_{1/2}O₂ obtained at 850, 900 and 950 °C decrease to 106, 140 and 86 mA·h/g after 50 cycles with the capacity retention of 43%, 58% and 55%, respectively. The sample obtained at 850 °C shows the highest initial specific discharge capacity as it is composed of nanoparticles with large surface area and short diffusion distance of sodium ion, but its capacity fades rapidly due to the poor crystallinity

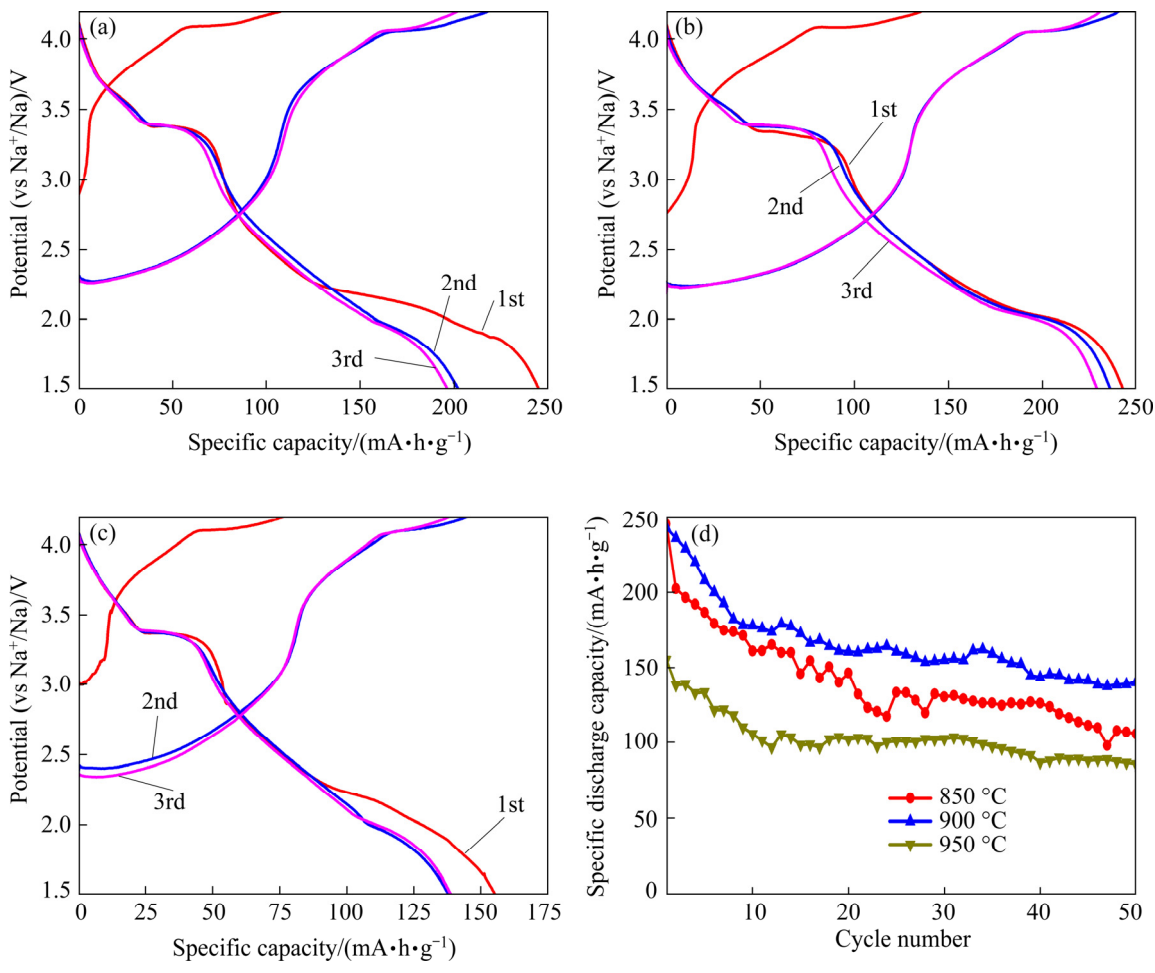


Fig. 5 First three charge-discharge curves of samples obtained at 850 °C (a), 900 °C (b) and 950 °C (c), and cycling performance of samples (d)

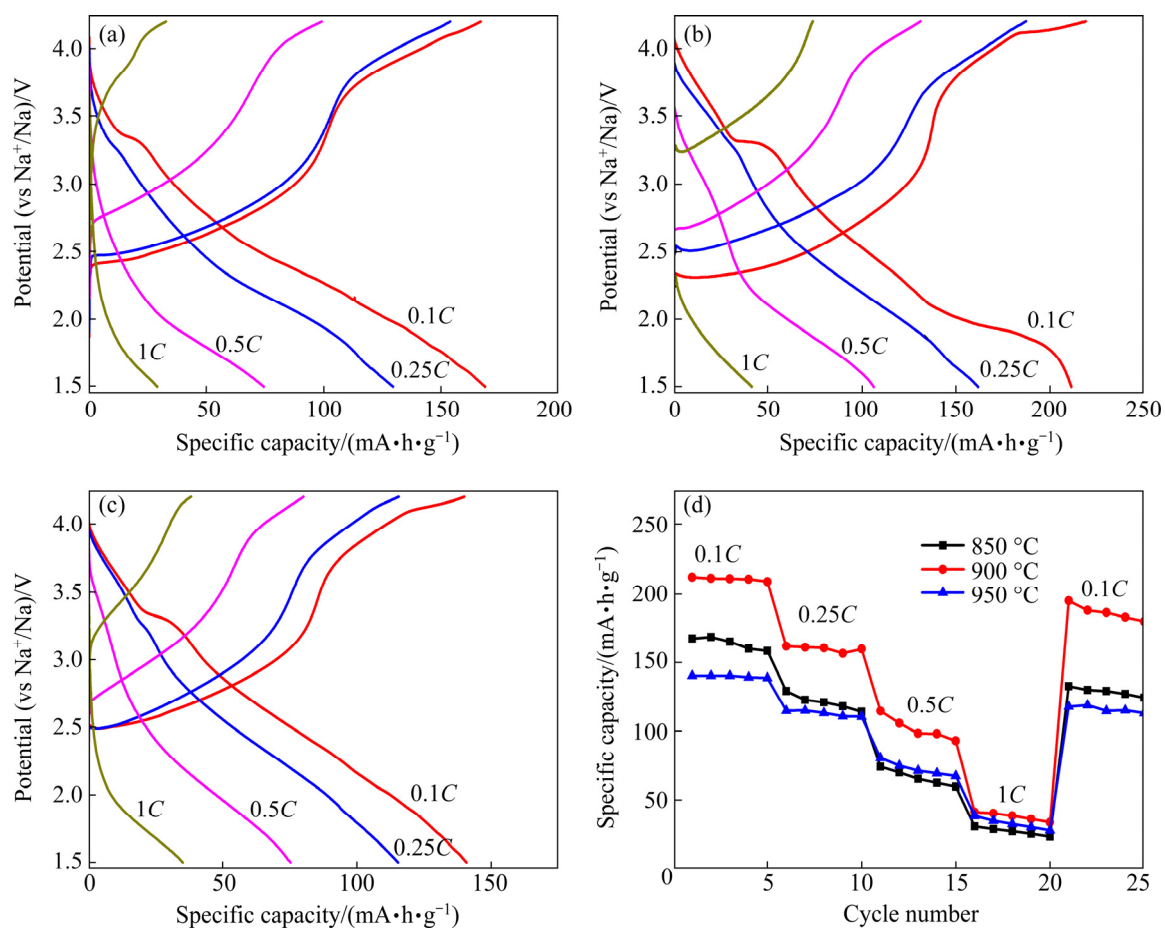


Fig. 6 Charge/discharge curves of samples obtained at 850 °C (a), 900 °C (b) and 950 °C (c) at various *C*-rates and rate performance of samples (d)

and the agglomeration of the nanoparticles. With increasing the temperature to 900 °C, the sample has better crystallinity and more uniform size distribution, resulting in better cycling performance. When the temperature increases to 950 °C further, the contact area between the active electrode material and electrolyte decreases and the diffusion distance of sodium ion increases as the average size of particles increases, which results in lower capacity. In addition, the P2-type Na_{2/3}Fe_{1/2}Mn_{1/2}O₂ reported in this work [16-26,29,31] shows the highest initial specific discharge capacity up to now, and the capacity fading is considerably smaller in comparison with other studies [20,21,23,25,29]. This should be attributed to the fact that the materials synthesized in this work are of hexagon plate-shape with the particle size of sub-micron.

Figure 6 plots the charge/discharge curves at various C-rates (1C= $260 \,\mathrm{mA/g}$) and the rate performance of samples obtained at different temperatures. The capacities of all samples gradually decay with increasing the current

densities. The sample obtained at 900 °C shows the highest specific capacities at various *C*-rates, which delivers the specific discharge capacities of 212, 162, 115 and 41 mA·h/g at 0.1*C*, 0.25*C*, 0.5*C* and 1*C*, respectively. When it is reversed back to 0.1*C* after 20 cycles, the sample still delivers a specific discharge capacity of 195 mA·h/g, indicating the good stability and structure reversibility of sample. However, the high rate performance of P2-type Na_{2/3}Fe_{1/2}Mn_{1/2}O₂ needs to be improved in our further study.

4 Conclusions

- (1) P2-type $Na_{2/3}Fe_{1/2}Mn_{1/2}O_2$ is successfully synthesized by a facile sol-gel method, and the calcination temperature has a significant effect on the morphology and electrochemical performance of the samples.
- (2) P2-type $Na_{2/3}Fe_{1/2}Mn_{1/2}O_2$ obtained at 900 °C is composed of hexagon plate-shaped particles with the size and thickness of 2–4 μm and

200-400 nm, respectively. It shows a high initial specific discharge capacity of 243 mA·h/g at a current density of 26 mA/g with good cycling stability.

Acknowledgments

The authors are grateful for the financial supports from the Natural Science Foundation of Hunan Province, China (No. 2020JJ5102), and the Scientific Research Fund of Hunan Provincial Education Department, China (No. 19A111).

References

- [1] SLATER M D, KIM D, LEE E, JOHNSON C S. Sodium-ion batteries [J]. Advanced Functional Materials, 2013, 23: 947–958.
- [2] HWANG J Y, MYUNG S T, SUN Y K. Sodium-ion batteries: Present and future [J]. Chemical Society Reviews, 2017, 46(12): 3529–3614.
- [3] YANG Shao-bin, DONG Wei, SHEN Ding, LI Si-nan, WANG Zhong-jiang, ZHANG Jia-min, SUN Wen, ZHANG Qin. Research progress of anode material for sodium-ion batteries [J]. The Chinese Journal of Nonferrous Metals, 2016, 26: 1054–1064. (in Chinese)
- [4] LV Wei-jun, HUANG Zhi-gao, YIN Ya-xia, YAO Hu-rong, ZHU Hai-liang, GUO Yu-guo. Strategies to build high-rate cathode materials for Na-ion batteries [J]. ChemNanoMat, 2019, 5: 1253–1262.
- [5] KIM H, KIM H, DING Z, LEE M H, LIM K, YOON G, KANG K. Recent progress in electrode materials for sodium-ion batteries [J]. Advanced Energy Materials, 2016, 6: 1600943.
- [6] FANG Yong-jin, XIAO Li-fen, CHEN Zhong-xue, AI Xinping, CAO Yu-liang, YANG Han-xi. Recent advances in sodium-ion battery materials [J]. Electrochemical Energy Reviews, 2018, 1: 294–323.
- [7] LIANG Shu-quan, CHENG Yi-bing, FANG Guo-zhao, CAO Xin-xin, SHEN Wen-jian, ZHONG Jie, PAN An-qiang, ZHOU Jiang. Research progress of key materials for energy photoelectric conversion and large-scale energy storage secondary batteries [J]. The Chinese Journal of Nonferrous Metals, 2019, 29: 2064–2114. (in Chinese)
- [8] QIN Mu-lan, LIU Wan-min, XIANG Yuan-jin, WANG Wei-gang, SHEN Bin. Synthesis and electrochemical performance of V₂O₅/NaV₆O₁₅ nanocomposites as cathode materials for sodium-ion batteries [J]. Transactions of Nonferrous Metals Society of China, 2020, 30: 2200–2206.
- [9] LUO Chao, LANGROCK A, FAN Xiu-lin, LIANG Yu-jia, WANG Chun-sheng. P2-type transition metal oxides for high performance Na-ion battery cathodes [J]. Journal of Materials Chemistry A, 2017, 5: 18214–18220.
- [10] WANG Sheng-han, SUN Cheng-lin, WANG Ning, ZHANG Qi-chun. Ni- and/or Mn-based layered transition metal oxides as cathode materials for sodium ion batteries: Status, challenges and countermeasures [J]. Journal of Materials

- Chemistry A, 2019, 7: 10138-10158.
- [11] CLÉMENT R J, BRUCE P G, GREY C P. Review: Manganese-based P2-type transition metal oxides as sodium-ion battery cathode materials [J]. Journal of The Electrochemical Society, 2015, 162: A2589–A2604.
- [12] SU Heng, JAFFER S, YU Hai-jun. Transition metal oxides for sodium-ion batteries [J]. Energy Storage Materials, 2016, 5: 116–131.
- [13] DELMAS C, FOUASSIER C, HAGENMULLER P. Structural classification and properties of the layered oxides [J]. Physica B+C, 1980, 99: 81–85.
- [14] JIA Min, QIAO Yu, LI Xiang, QIU Fei-long, CAO Xin, HE Ping, ZHOU Hao-shen. Identifying anionic redox activity within the related O3- and P2-type cathodes for sodium-ion battery [J]. ACS Applied Materials & Interfaces, 2020, 12(1): 851–857.
- [15] ZHU Hong-li, LEE K T, HITZ G T, HAN Xiao-gang, LI Yuan-yuan, WAN Jia-yu, LACEY S, WALD CRESCE A, XU Kang, WACHSMAN E, HU Liang-bing. Free-standing Na_{2/3}Fe_{1/2}Mn_{1/2}O₂@graphene film for a sodium-ion battery cathode [J]. ACS Applied Materials & Interfaces, 2014, 6: 4242–4247.
- [16] CHEN Jia-bin, ZHONG Sheng-kui, ZHANG Xiao-ping, LIU Jie-qun, SHI Shao-nan, HU Yong, WU Ling. High performance of hexagonal plates P2-Na_{2/3}Fe_{1/2}Mn_{1/2}O₂ cathode material synthesized by an improved solid-state method [J]. Materials Letters, 2017, 202: 21–24.
- [17] YABUUCHI N, KAJIYAMA M, IWATATE J, NISHIKAWA H, HITOMI S, OKUYAMA R, USUI R, YAMADA Y, KOMABA S. P2-type Na_x[Fe_{1/2}Mn_{1/2}]O₂ made from earth-abundant elements for rechargeable Na batteries [J]. Nature Materials, 2012, 11: 512–517.
- [18] ILARDUYA J M D, OTAEGUI L, AMO J M L D, ARMAND M, SINGH G. NaN₃ addition, a strategy to overcome the problem of sodium deficiency in P2-Na_{0.67}[Fe_{0.5}Mn_{0.5}]O₂ cathode for sodium-ion battery [J]. Journal of Power Sources, 2016, 337: 197–203.
- [19] PARK J K, PARK G G, KWAK H H, HONG S T, LEE J W. Enhanced rate capability and cycle performance of titanium-substituted P2-type Na_{0.67}Fe_{0.5}Mn_{0.5}O₂ as a cathode for sodium-ion batteries [J]. ACS Omega, 2018, 3: 361–368.
- [20] PARK K, HAN D, KIM H, CHANG W S, CHOI B, ANASS B, LEE S. Characterization of a P2-type chelating-agentassisted Na_{2/3}Fe_{1/2}Mn_{1/2}O₂ cathode material for sodium-ion batteries [J]. RSC Advances, 2014, 4: 22798–22802.
- [21] KALLURI S, SENG K H, PANG W K, GUO Zai-ping, CHEN Zhi-xin, LIU Hua-kun, DOU shi-xue. Electrospun P2-type Na_{2/3}Fe_{1/2}Mn_{1/2}O₂ hierarchical nanofibers as cathode material for sodium-ion batteries [J]. ACS Applied Materials & Interfaces, 2014, 6: 8953–8958.
- [22] GUAN Miao, CHEN Jia-bin, ZHANG Xiao-ping, YANG Liu, WANG Bin-jue, ZHONG Sheng-kui. Yarn-ball-shaped P2-Na_{2/3}Fe_{1/2}Mn_{1/2}O₂ nanofibers prepared by magnetic-assisted electrospinning method as high-performance cathode material for Na-ion batteries [J]. Materials Letters, 2019, 254: 24–27.
- [23] XU Jian-tie, CHOU Shu-lei, WANG Jian-li, LIU Hua-kun, DOU Shi-xue. Layered P2-Na_{0.66}Fe_{0.5}Mn_{0.5}O₂ cathode material for rechargeable sodium-ion batteries [J].

ChemElectroChem, 2014, 1: 371-374.

- [24] PANG W K, KALLURI S, PETERSON V K, SHARMA N, KIMPTON J, JOHANNESSEN B, LIU Hua-kun, DOU Shi-xue, GUO Zai-ping. Interplay between electrochemistry and phase evolution of the P2-type Na_{2/3}Fe_{1/2}Mn_{1/2}O₂ cathode for use in sodium-ion batteries [J]. Chemistry of Materials, 2015, 27(8): 3150–3158.
- [25] BAI Ying, ZHAO Li-xiang, WU Chuan, LI Hui, LI Yu, WU Feng. Enhanced sodium ion storage behavior of P2-type Na_{2/3}Fe_{1/2}Mn_{1/2}O₂ synthesized via a chelating agent assisted route [J]. ACS Applied Materials & Interfaces, 2016, 8: 2857–2865.
- [26] KONG Wei-jin, YANG Wen-yun, NING De, LI Qing-yuan, ZHENG Li-rong, YANG Jin-bo, SUN Kai, CHEN Dong-feng, LIU Xiang-feng. Tuning anionic/cationic redox chemistry in a P2-type Na_{0.67}Mn_{0.5}Fe_{0.5}O₂ cathode material via a synergic strategy [J]. Science China: Materials, 2020, 63: 1703–1718.
- [27] SUI Yu-lei, HAO Yue-ying, ZHANG Xiao-ping, LI Jiang-peng, WEN Gong-yu, ZHONG Sheng-kui, ZHANG Zi-wei, WU Ling. Improved electrochemical properties of vanadium substituted Na_{0.67}Fe_{0.5}Mn_{0.5}O₂ cathode material for

- sodium-ion batteries [J]. Ceramics International, 2021, 47(4): 5227–5234.
- [28] QIN Mu-lan, LIU Wan-min, LIANG Shu-quan, PAN An-qiang. Facile synthesis of porous LiNiVO₄ powder as high-voltage cathode material for lithium-ion batteries [J]. Transactions of Nonferrous Metals Society of China, 2016, 26: 3232-3237.
- [29] VISWANATHA R, KISHORE B, BHARATH U, MUNICHANDRAIAH N. Communication: Electrochemical investigation of plate-like Na_{2/3}Fe_{1/2}Mn_{1/2}O₂ for sodium ion cathode [J]. Journal of The Electrochemical Society, 2018, 165: A263–A265.
- [30] TALAIE E, DUFFORT V, SMITH H L, FULTZ B, NAZAR L F. Structure of the high voltage phase of layered P2-Na_{2/3-z}[Mn_{1/2}Fe_{1/2}]O₂ and the positive effect of Ni substitution on its stability [J]. Energy & Environmental Science, 2015, 8: 2512–2523.
- [31] SUI Yu-lei, HAO Yue-ying, ZHANG Xiao-ping, ZHONG Sheng-kui, CHEN Jia-bin, LI Jiang-peng, WU-Ling. Spray-drying synthesis of P2-Na_{2/3}Fe_{1/2}Mn_{1/2}O₂ with improved electrochemical properties [J]. Advanced Powder Technology, 2020, 31: 190–197.

高容量钠离子电池正极材料 P2 型 $Na_{2/3}Fe_{1/2}Mn_{1/2}O_2$ 的简便合成

秦牡兰, 尹常宇, 许 稳, 刘 洋, 文俊豪, 申 斌, 王伟刚, 刘万民

湖南工程学院 材料与化工学院 环境催化与废弃物再生化湖南省重点实验室,湘潭 411104

摘 要:通过简单的溶胶凝胶法合成 P2 型 $Na_{2/3}Fe_{1/2}Mn_{1/2}O_2$ 正极材料并研究煅烧温度对材料结构、形貌和电化学性能的影响。结果表明,在 900 °C 煅烧得到的产物是高结晶度的 P2 型 $Na_{2/3}Fe_{1/2}Mn_{1/2}O_2$ 化合物且具有六角板状颗粒形貌,颗粒宽度为 $2\sim4$ μ m,厚度为 $200\sim400$ nm。样品以 26 mA/g 充放电时表现出 243 mA·h/g 的初始放电比容量和良好的循环性能,其高容量说明 P2 型 $Na_{2/3}Fe_{1/2}Mn_{1/2}O_2$ 是一种很有应用前景的钠离子电池正极材料。 关键词: 钠离子电池; 正极材料; $Na_{2/3}Fe_{1/2}Mn_{1/2}O_2$; 电化学性能; 溶胶凝胶法

(Edited by Bing YANG)